Journal of Structural Geology 31 (2009) 628–636

Contents lists available at ScienceDirect

Journal of Structural Geology

journal homepage: www.elsevier.com/locate/jsg

The spatial heterogeneity of structures in high porosity sandstones: Variations and granularity effects in orientation data

Jiulin Guo [a,*], Kenneth McCaffrey [a], Richard Jones [b], Robert Holdsworth [a]

[a] Reactivation Research Group, Department of Earth Sciences, Durham University, Durham DH1 3LE, UK
[b] Geospatial Research Ltd, Earth Sciences, Durham University, UK

ARTICLE INFO

Article history:
Received 25 April 2008
Received in revised form
17 December 2008
Accepted 21 December 2008
Available online 18 January 2009

Keywords:
Geospatial analysis
Spatial variation
Fracture heterogeneity
Spatial aliasing
Deformation bands

ABSTRACT

Despite many studies on the scaling and geometrical properties of fracture systems, much less attention has been paid to analysing their spatial characteristics. At a well exposed section at George Gill, Appleby, we investigated the spatial heterogeneity in deformation band orientations in a high porosity sandstone using bootstrap, variogram and hierarchical analysis methods. At metre-scales the structures displayed multimodal orientation patterns with orthorhombic symmetry whereas at 20 m scales they appeared bimodal. Our analysis shows that this situation arises due to a combination of small-scale noise superimposed on a regional trend related to the presence of a nearby major fault structure. We suggest that this type of geospatial analysis can be used as a general tool to investigate spatial heterogeneity in structural systems. We also suggest that these types of granularity and aliasing effect impact the prediction and modelling of rock properties and they therefore warrant further investigation.

1. Introduction

Our knowledge of the three dimensional (3D) characteristics of fracture networks is limited due to their inherent complexity, which results from their initiation and mutual interaction, and from constraints imposed by the incomplete sampling of rock volumes. The prediction of rock properties such as permeability, strength, seismic velocity and anisotropy in the Earth's subsurface, however, requires a complete understanding of the geometry and spatial attributes of fracture networks (e.g. Crampin et al., 1980; Barton and Zoback, 1992; Laubach et al., 2004; Philip et al., 2005; Ortega et al., 2006). Currently the model inputs for fractured hydrocarbon reservoirs and aquifers necessitate the characterization of fracture geometries, sizes and spatial properties at a range of scales (Fig. 1). These data are generated from well logs and core (one dimensional (1D), centimetre resolution), seismic attribute mapping (two dimensional (2D), tens-of-metres), and analogue outcrops (2D data at centimetre scales) (e.g. Gillespie et al., 1993). In this paper, we present a methodology that can be used to investigate the spatial heterogeneity of structures in a deformed host rock. Where we use the term 'fracture', we are referring in a general sense to any planar discontinuous surfaces or zones (such as joints, faults and deformation bands) generated by brittle deformation processes. The example given in this paper is a dataset collected from a high porosity sandstone outcrop and here we use the term 'deformation band' in a specific sense to refer to structures in the case study.

The attributes of fracture systems visible at different resolutions typically form a 'hierarchy' (Fig. 2). '*Granularity*' in a general sense refers to the relative size, scale, level of detail or depth of penetration that characterizes an object or activity (Zadeh, 1979). In this study, we illustrate the importance of granularity effects in analysing a fracture dataset collected from a natural system. This effect is not the same as scaling which is the extent to which structures are similar at different scales of observation and has been widely investigated for various dimensional and spatial properties for fractures (c.f. Bonnet et al., 2001).

The problem we initially encountered was that when viewed at the first-order hierarchical level (the complete deformation band dataset in this example), the orientation patterns seemed relatively simple, i.e. two clusters that are NE- and SW-dipping respectively. However, in most parts of the outcrop at metre-scale (a lower hierarchical level), we observed more complexity, with three or more orientation clusters developed.

In this paper, using a variety of statistical analyses, we demonstrate that substantial local scale variation in orientation is superimposed on overall trends at the scale of the outcrop as a whole. Our results show that spatial heterogeneity in fracture orientations

* Corresponding author.
E-mail addresses: jiulin.guo@yahoo.co.uk (J. Guo), k.j.w.mccaffrey@durham.ac.uk (K. McCaffrey).

0191-8141/$ – see front matter © 2009 Elsevier Ltd. All rights reserved.
doi:10.1016/j.jsg.2008.12.002

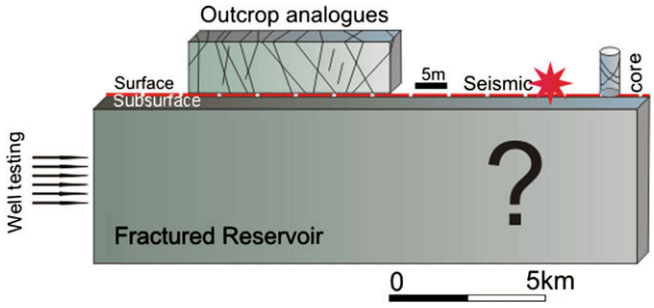

Fig. 1. Schematic diagram illustrating the techniques used to study fracture networks at different scales. All this information is required to predict the complete fracture network in three dimensions in the subsurface.

can be delineated by analysing the fractures at different resolutions, provided the locations of individual structures are also recorded. In our example, if the data are averaged at a coarse scale then important characteristics of the fracture system remain hidden. This granularity effect causes a type of spatial aliasing that is known in other systems (e.g. seismic processing, time series analysis) and requires explicit understanding if more realistic prediction of natural fracture network geometries is to be successfully made in the subsurface.

2. Geological background

We studied an outcrop of fractured aeolian red sandstone that occurs in the Permo-Trias Vale of Eden half graben at George Gill, Appleby, located east of the English Lake District and 20 km SE of Penrith (Fig. 3, NY716190), (Versey, 1938). Cataclastic deformation bands and deformation band clusters are well developed along both sides of a stream valley. Anastomosing deformation bands are ubiquitous and are best displayed on a 40-m long, south-facing cliff on the northern side of the valley (Figs. 3 and 4a). The host sandstone preserves widespread cross-bedding, is highly porous and poorly cemented, whereas the deformation bands (and deformation band clusters) are much finer grained, better cemented, and have lower porosity. As these low-porosity deformation bands can act as preferential groundwater flow paths, the orientation, continuity and physical connectivity of the bands determines their effectiveness as sealing or flow-reducing structures (Sigda et al., 1999; Fossen et al., 2007).

Deformation band density changes abruptly approximately 20-m from the eastern end of the cliff (Fig. 4a). A single deformation band is a narrow zone of grain fragments (ca. 1 mm), representing a single slip event with a small displacement; a deformation band cluster is formed by coalescence of single deformation bands (Aydin and Johnson, 1978). Both single deformation bands and deformation band clusters display a diffuse bimodal distribution pattern on stereonets (Fig. 4a and b). In the zone of low fracture density toward the east, three (multimodal) sets of mutually cross-cutting fractures in the form of single deformation bands can be recognized in the field (Fig. 4b and c). They are similar to the arrays of deformation bands in the Entrada and Navajo sandstones in southeastern Utah, where the faults form a network that usually has a rhombohedral pattern (e.g. Aydin and Reches, 1982; Shipton and Cowie, 2001; Johansen and Fossen, 2008). In the high density zone, the deformation band clusters almost obliterate the host rock entirely (Fig. 4d). Viewed as a whole, the deformation band clusters appear to be distributed into two broad groups (bimodal) striking generally NW–SE and dipping moderately to steeply either SW or NE (Fig. 4a). Sub-horizontal beds are offset across deformation bands in the low density zone typically by 1–2 cm at most, and by around 5 cm in the high density zone. Rare slickenlines found on a fracture plane beneath the cave are dip-slip, plunging SW (Fig. 4a and e). At other localities along Hilton Beck near Red Brow (NY708201), 1 km NW from George Gill, slickenlines are more commonly developed on the polished fault surfaces, and also show a dip-slip normal sense (Fig. 3). Faults that exhibit slickenlines around Hilton Beck and George Gill generally trend NW–SE, suggesting a regional NE–SW extension.

At the microscale, the host rock consists of ca. 80% quartz and ca. 10% feldspar grains, most of which are rounded and loosely packed (Fig. 5a). Cementation in the host rock is mainly due to pressure solution that occurred along the contacts between adjacent grains. In the inner zones of single (ca. 1 mm wide) deformation bands, grains are rotated, ruptured and more tightly packed than in the host rock (Fig. 5b). The offset for a given single deformation band is generally not obvious as simple discontinuities with offset grain fragments are absent. Slip surfaces can, however, occur within bands or, more commonly, along or within zones of multiple deformation bands, representing a more mature development stage for the deformation bands (Fossen et al., 2007). In deformation band clusters (ca. 5 cm width), the original grains are intensively brecciated to form very highly compacted cataclasites. Shear

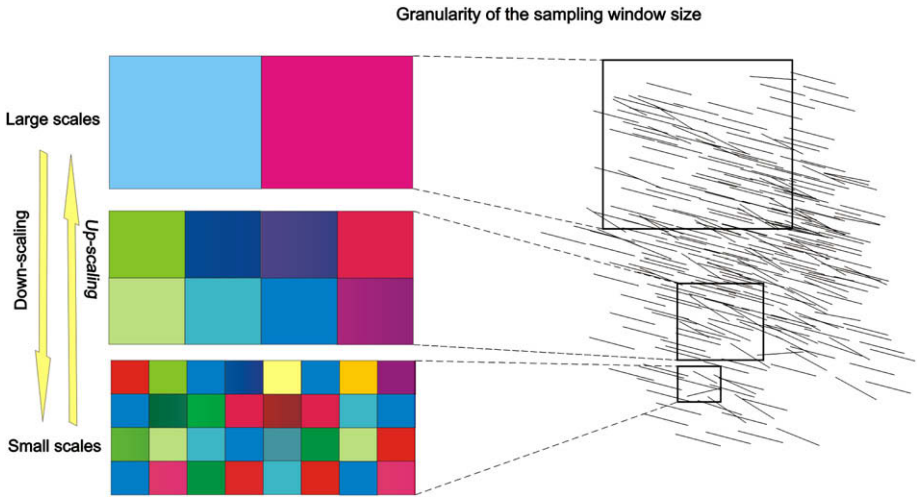

Fig. 2. Schematic diagram illustrating the granularity of a sampling window system. The colour maps show a hierarchical relationship between measurements from different sampling window sizes: the greater variety of colour at smaller scales compared with that at larger scales illustrates greater variation. Lines on the right are a schematic fracture network that is sampled at different window sizes shown as black boxes.

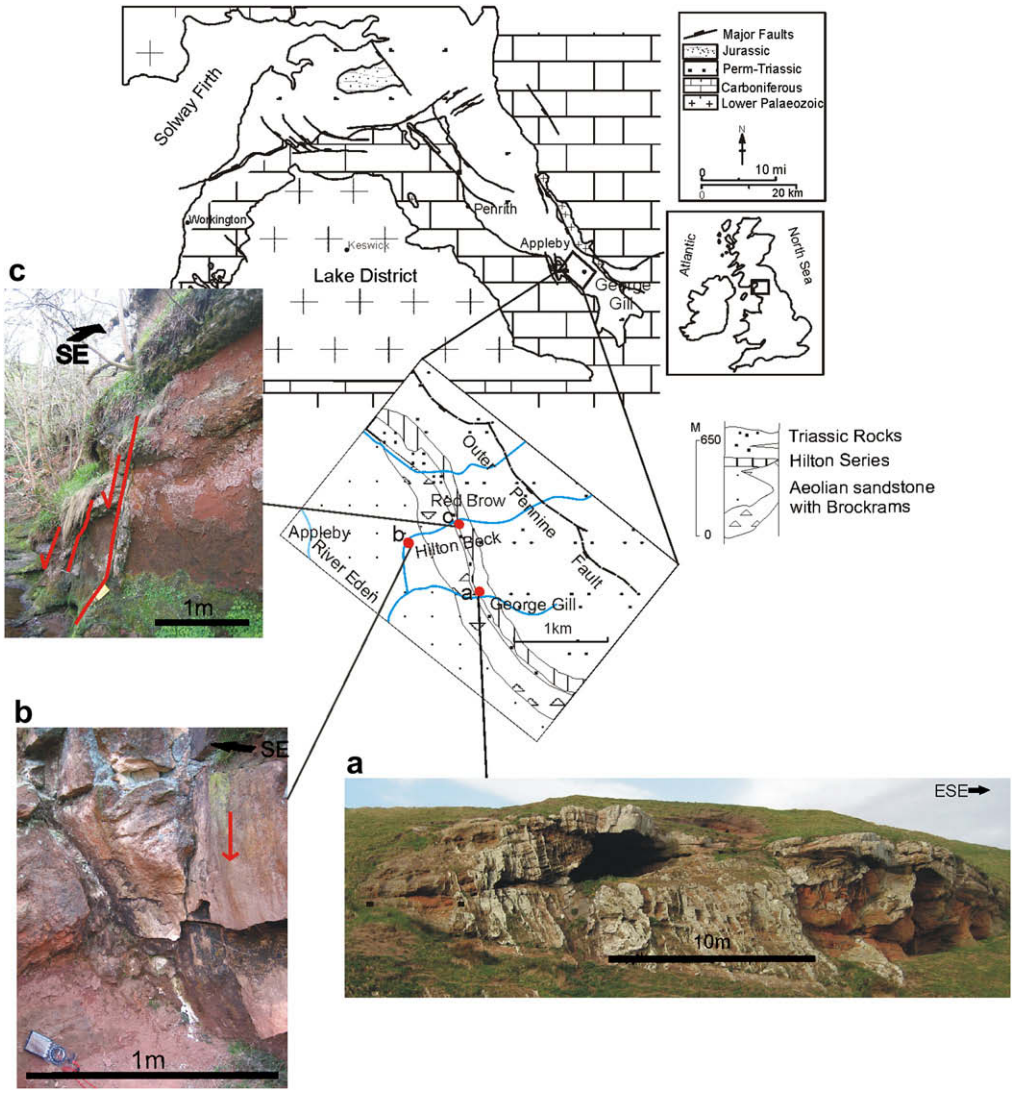

Fig. 3. Regional geological map of the Penrith area showing the location of Appleby where Permian aeolian sandstone with basal brockrams (breccias) underlying thin-bedded muddy sand (Hilton Series) and Triassic rocks (detailed map) is exposed (after Versey, 1938). (a) Locality a: a ≈ 40 m long cliff with anatomising deformation bands in the northern side of the stream valley at George Gill. (b) and (c) Outcrop-scale normal faults trending NW–SE along Hilton Beck shown on the detailed map preserve (see detailed map) expose well-defined dip-slip slickenlines on the exposed fracture surfaces of the deformation bands.

is localized in narrow zones (≈1 mm width) (Fig. 5c). The characteristics of the deformation bands from Appleby closely resemble deformation bands described in other regions (e.g. Underhill and Woodcock, 1987; Antonellini et al., 1994; Johansen and Fossen, 2008). Overall, in terms of deformation intensity, the deformation band clusters are consistent with the three-fold division of fault evolution in highly porous sandstones described by Aydin and Johnson (1978).

3. Methodology and results

To investigate the spatial variability and directional anisotropy in fracture datasets, each fracture orientation measurement is described by its position in a geographic or a Cartesian reference frame (Isaaks and Srivastava, 1989). Despite the large body of work concerning the statistics of directional (orientation) data (e.g. Fisher et al., 1987; Mardia and Jupp, 2000), *spatial heterogeneity* in fracture datasets has not been considered in as great a detail. This situation is surprising since systematic changes in fracture orientations could, for example, indicate rotations in palaeostress axes (e.g. Faulkner et al., 2006). More generally, an understanding of fracture orientation with respect to spatial position in a rock unit is part of a complete description of a fracture network.

In this study, we investigated 3 distinct aspects of spatial heterogeneity in the deformation-band-orientation dataset: (1) *geometrical clustering*; (2) *spatial correlation*; and (3) *spatial variation*. In this study, *geometrical clustering* refers to clusters in deformation band orientations from location to location along the outcrop. *Spatial correlation* describes the similarity of any two orientation measurements separated by certain distances. *Spatial variation* describes the change in orientation with spatial location. We use three corresponding techniques to study each of these distinct aspects: (1) *bootstrapping*; (2) *semivariograms*; and (3) *hierarchical analysis*.

3.1. Data acquisition and manipulation

We collected approximately 950 deformation band orientations in 1 m sized windows along a 1D scanline across the George Gill outcrop to form a data log. The location of each sampling window is

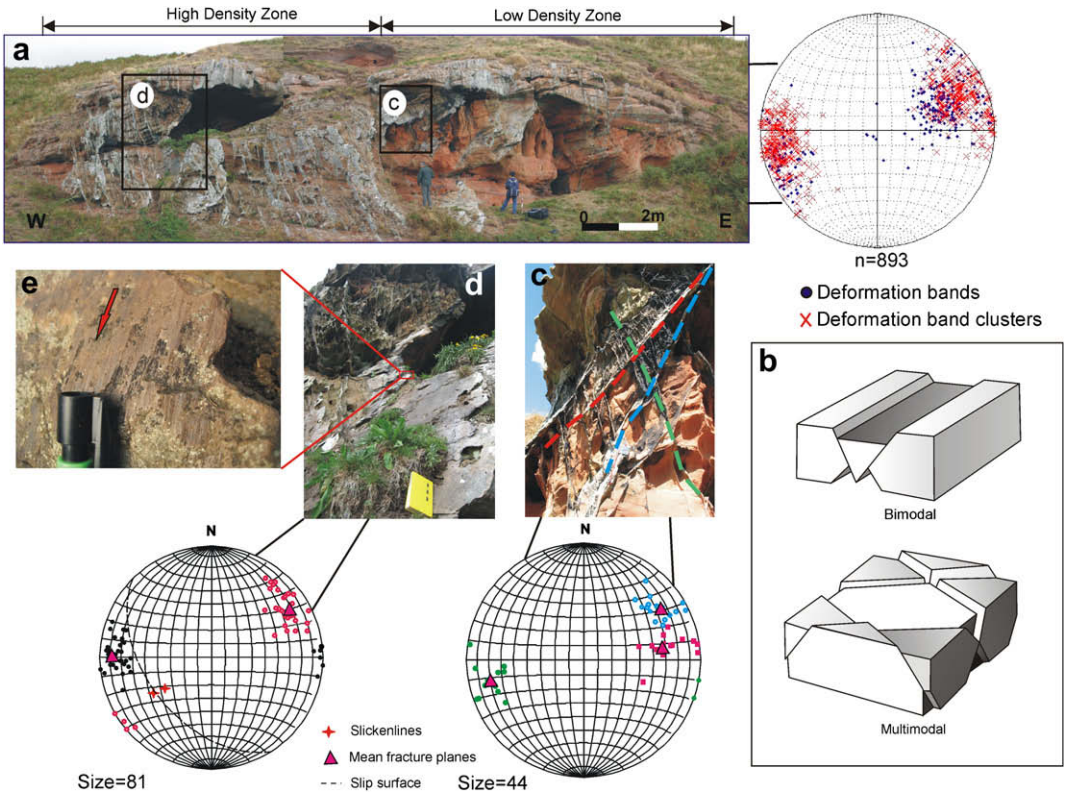

Fig. 4. Deformation bands and deformation band clusters on the south-facing cliff at George Gill. (a) Overview of the cliff section showing the density change in the middle of the outcrop with the low density zone of mainly single deformation bands on the right; the high density zone of mainly deformation band clusters on the left, and locations of insets c and d shown. (b) Block diagram illustrating bimodal and multimodal fracture patterns. (c) Locally developed multimodal deformation with three sets of cross-cutting planes. These different sets are correspondingly shown in open circles, dots and squares on the stereonets with mean values (below) for the different sets in triangles. (d) Fault plane with slickenlines (shown in (e)) indicating dip-slip displacement. Two fault sets in open circles and dots are shown on the attached stereonets. All stereoplots are Schmidt projection, lower hemisphere.

defined by the distance from the east end of the cliff to the centre of the window (Fig. 6a). Orientation datasets were collected in the sample windows using a compass-clinometer moving sequentially from east to west along the cliff (Fig. 6b). Measurements from the same sampling window are allocated the same spatial location as the window. Orientations were recorded directly onto digital photographs using a Tablet PC (e.g. Clegg et al., 2006) to locate the precise position of the measurement on the outcrop. The fracture density is defined as the number of entire or partial traces recorded in the 1×1 m sampling window. In the low density zone, all accessible deformation bands were measured in a sampling window so that the sample size reflects the fracture density (Fig. 6c). In the high density zone, the occurrence of deformation band clusters precluded accurately counting the number of bands and establishing a complete set of orientation measurements. So, a representative sample size was obtained by sufficiently collecting orientation data in a sampling window. Additionally, for curving deformation bands, more than one measurement was taken to record changes in orientation.

Deformation bands in the relatively homogeneous sandstone exhibit a broadly conjugate pattern at the outcrop-scale, with two diffuse clusters plotting in the NE and SW quadrants of the stereonet (Fig. 4a). Therefore we subdivide the dataset into two major sets (NE-dipping and SW-dipping sets) as a function of orientation. To further resolve the correlation of changes in orientation to spatial position, we statistically describe the spatial heterogeneity of the orientation population for the bands.

3.2. Bootstrap analysis

Bootstrap analysis is a statistical method for estimating the sampling distribution of an estimator by sampling with

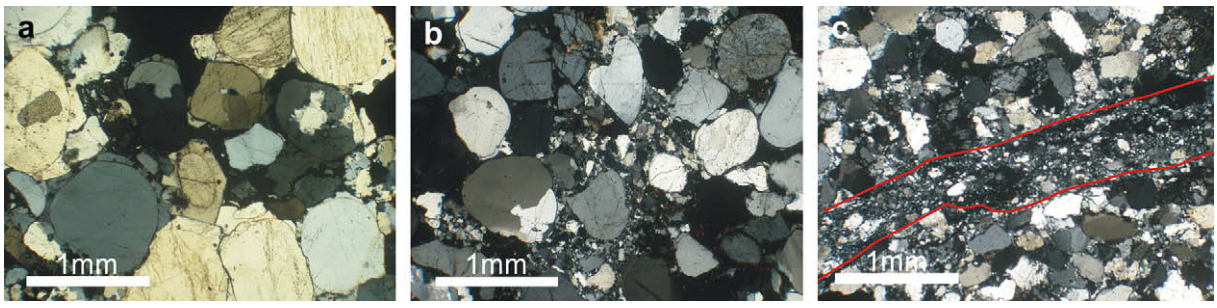

Fig. 5. Thin sections of: (a) host rock, (b) inner zones, and (c) localized shear in narrow zones. CPL.

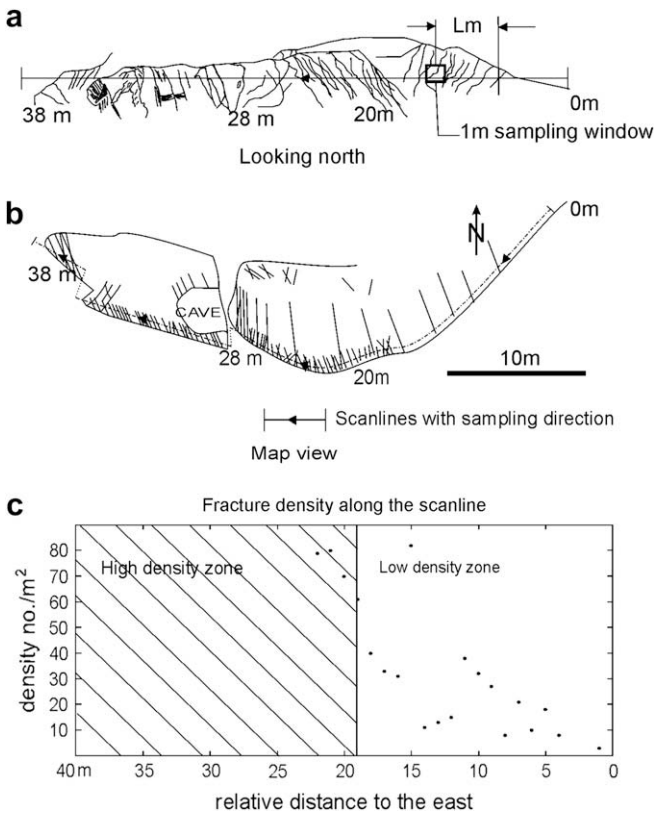

Fig. 6. (a) Sketch section (looking N) of the cliff at George Gill showing a typical 1 m sampling window, which was moved sequentially westward relative to the sample line origin in the east (0 m). The curvilinear traces represent deformation bands/clusters (b) Map view showing the scanline dotted along the cliff base. The liner traces represent deformation bands/clusters. (c) Plot of deformation band density vs. distance from the east end of the cliff showing that the density increases toward the western end. The shaded area indicates zone of high density (generally > fractures $90m^{-2}$).

replacement from the original sample (Efron, 1982). The technique is particularly useful for analysing diffuse orientation data (Mardia and Jupp, 2000). A simple diagram showing stereoplots of fracture orientations versus their spatial location along a scanline can resolve variations in datasets with large spatial heterogeneities (e.g. Wilson et al., 2006). However, if the variation within a set of fracture orientations is large, the spatial heterogeneity can be masked as occurs at George Gill (Fig. 4a). Bootstrap analysis is a robust technique that can recognize the spatial heterogeneity when such variation occurs.

To investigate geometric clustering in the orientation datasets, sequentially bootstrapped means are compared with randomly bootstrapped means determined by using a moving window. A 'moving window' is defined as a sub-dataset made from measurements adjacent to each other in the data log. We calculated the vector mean (e.g. Mardia and Jupp, 2000) in a 'moving window' starting from the beginning of the data log, corresponding to the east end of the cliff, and repeated the same operation on orientation measurements working progressively toward the end of the data log (corresponding to the west end of the cliff). Whereas in the field the 'sampling window' locations were stepped by 1 m increments, in the bootstrap analysis, we use a 'moving window' with a step of one orientation measurement in the data log to highlight planes of similar orientations in a spatially correlated context. Finally, we calculated the mean orientations using spherical data analysis (Mardia and Jupp, 2000) of similar sized samples selected at random from the whole dataset (i.e. ignoring the spatial position of the measurements). This process was repeated many times, for a series of different 'moving window' sizes. If *spatial clustering* exists in the datasets, the sequentially bootstrapped means will show different behaviour compared to the randomly bootstrapped means. This difference is shown by plotting the means on stereonets (Fig. 7).

The relationship between the spatial position and the deformation band orientation was also analyzed using a 'moving window bootstrap': a simulation was launched in each 'moving window' to generate pooled mean orientations that were colour-coded from a greyscale (the colour is determined by the spatial position of the 'moving window') to estimate the spatial variation (Fig. 8). This simulation is somewhat analogous to the sampling windows used in the field: orientations are sampled in a window that moves across the datasets. However, unlike in the field, this approach defines the window size using the number of orientation data that occur immediately adjacent to each other to form a sub-dataset in which the random sampling is applied for a large number of repetitions. The window moves with an overlap of only 1 different measurement with each step. Given the degree of overlap, a reasonable expectation is that proximal datasets will have similar bootstrap estimates.

Stereoplots illustrate that substantial variations of deformation band orientation exist for both the NE- and SW-dipping sets. The sequentially bootstrapped means vary in an approximately 20° range (Fig. 7a). The NE-dipping set varies substantially in the horizontal plane (i.e. there is more variation in strike than dip), whilst the SW-dipping set varies substantially in the vertical plane (i.e. dip varies more than strike) (Fig. 7a). Fig. 8 shows that the deformation bands in both the NE- and SW-dipping sets rotate systematically as the location moves from east to west across the cliff. NE-dipping deformation bands vary clockwise (looking down) in a horizontal plane whereas the SW-dipping set becomes steeper, with both showing changes of approximately 20°. By contrast, the random bootstrapped means reveal two sets of tight clusters on the NE and SW side of the stereonet respectively (Fig. 7b), which approximately follow a Fisher distribution model (Fisher et al., 1987). The results suggest that a smaller 'moving window' will reveal more variable local estimates, which, as shown, remains hidden in a larger 'moving window', although the trend from both Figs. 7 and 8 are not sensitive to changing sampling size (Figs. 7a and 8a–c), suggesting a fairly strong heterogeneity in the spatial variation of the dataset. Given that both the orientation and deformation band morphology change from east to west, single deformation bands differ in orientation from band clusters.

3.3. Semivariograms

The semivariance, $\widehat{\gamma}(h)$ is used to quantify the spatial correlation for spatially distributed datasets and is the basis for all geostatistical methods (La Pointe and Hudson, 1985; Isaaks and Srivastava, 1989).

$$\widehat{\gamma}(h) = \frac{1}{2N(h)} \sum_{||xi-xj|| \approx h} \left|\left|Z(x_i) - Z(x_j)\right|\right|^2 \quad (1)$$

where $Z(x_i)$ and $Z(x_j)$ are the observations at locality x_i and x_j, respectively. $N(h)$ describes the number of pairs of observations at these localities separated by the lag h defined as $\|x_i - x_j\|$. Semivariograms generated by plotting h against $\widehat{\gamma}(h)$ illustrate the degree of spatial correlation in the data. For spatially heterogeneous datasets, closely spaced measurements are expected to have a higher correlation compared to measurements spaced further apart. In this study, it is important to define a suitable parameter to represent the difference between two geographically separated measurements, because the orientation data are bivariables and can be illustrated as vectors distributed on a unit sphere. Hence, the

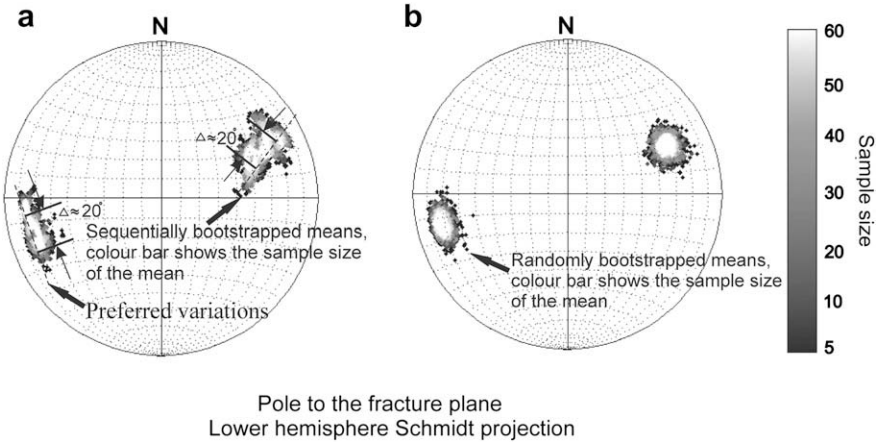

Fig. 7. Results of bootstrap analysis. (a) Sequentially bootstrapped means in the NE and SW set. Dashed lines are the preferred ≈20° variations observed for each set. Greyscale bar indicates the sample size of the mean. (b) Randomly bootstrapped means in the NE and SW sets each with a tight cluster.

difference between two measurements cannot be adequately represented by simply subtracting one from another. Instead, we use the angular difference between the poles to fracture planes to describe their dissimilarity (e.g. La Pointe, 1993). Equation (1) was therefore modified for calculating the semivariance to reveal the spatial correlation in the orientation dataset thus:

$$\widehat{\gamma}(h) = \sqrt{\frac{1}{2N(h)} \sum_{\|xi-xj\| \approx h} \text{angular}\left(Z(x_i), Z(x_j)\right)^2} \qquad (2)$$

where angular $(Z(x_i), Z(x_j))$ is the acute angle between the poles to two fracture planes measured in the plane normal to their mutual intersection; $\|x_i - x_j\| \approx h$ represents any pairs of fractures separated by the geographical distance h; $N(h)$ is the total number of pairs of fractures whose geographical distance is determined by $\|x_i - x_j\| \approx h$. Semivariograms include several important features. For example, as the separation distance between pairs of measurements increases, the corresponding semivariance will also generally increase. Eventually, an increase in the separation distance no longer causes a corresponding increase in the semivariance and the semivariogram reaches a plateau. The distance (lag h) at which the semivariogram reaches this plateau is called the *range*. The plateau reached by the semivariogram at the range is called the *sill*. When the semivariance reaches the sill, measurements separated by the corresponding distance are no longer spatially correlated. Finally, whilst the value of the semivariogram for $h = 0$ is strictly 0, several factors, such as sampling error and small-scale variability, may cause sample values separated by extremely small distances to be dissimilar. The jump from zero at the origin to the semivariance at extremely small distances is called the *nugget effect* (Isaaks and Srivastava, 1989)

The semivariance calculated from the deformation band orientation data (Fig. 9) shows that the nugget effect for the whole dataset (NE- and SW-dipping sets combined) is around 17°, suggesting that fracture orientations measured close to each other vary in the range of ca. 34° (i.e. twice the semivariance). This is substantially larger than for each of the sets (NE- and SW-dipping) where the average angular difference between two closely separated fractures in the NE- and SW-dipping sets is about 19° and 23° (twice their semivariance) respectively, showing that each set has noticeable variation. As the deformation bands here are mutually cross-cutting, these results can be interpreted to be the result of locally developed multimodal brittle deformation (Fig. 4), (c.f. Faulkner et al., 2006). The semivariance linearly increases with lag h before reaching the limits where high fluctuations are due to a lack pairs of measurements separated by a large distance (shown in the shaded area in Fig. 9). It appears that the deformation bands have a strong spatial correlation up to at least the 25 m scale.

3.4. Hierarchical analysis

To investigate the granularity effects in the orientation dataset, we increased the size of sampling windows by combining our

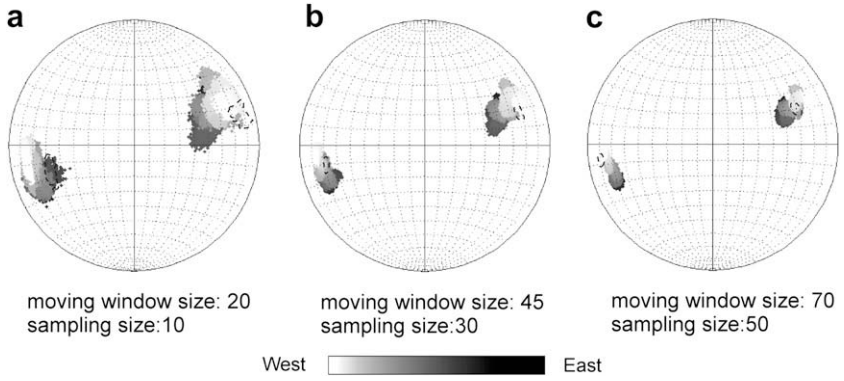

Fig. 8. Spatial variation in deformation band orientation from the 'moving window' bootstrap analysis. The greyscale bar shows the spatial location from the east to the west of the cliff. A large number of bootstrapped orientations from a 'moving window' will be allocated the same grey when they are plotted on the stereonets. (a)–(c) Results of the 'moving window bootstrapping' as a function of window and sample size.

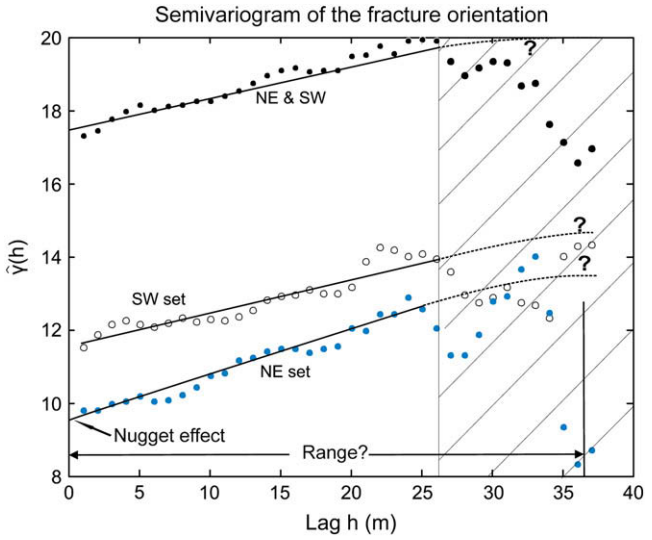

Fig. 9. Semivariogram of the deformation band orientation. The distance (lag h) separating any two measurements shows a strong positive correlation with semivariance. In the whole dataset, the nugget effect is ≈17°. In the NE- and SW-dipping sets, the nugget effect is ≈9.5° and ≈11.5°. Shaded area is the region where the sill and range are difficult to determine due to limited number of pairs of measurements.

datasets into different sampling window sizes to form a hierarchy of observations, from small (e.g. metre-scale) to relatively large (tens-of-metre) scales (cf. Fig. 2). This analysis gives a tool to gain insights into the spatial variation of the orientations over the available scale-range. We chose 3 m, 5 m, 10 m and 20 m scales to investigate the patterns of spatial variation in this 40 m long cliff. Upscaling is realized by combining the original 1 m sampling windows into progressively larger window sizes. Measurements at 3 m scale, for example, are simply a combination of three adjacent 1 m sampling windows. We can calculate the standard errors of the mean from different windows of the same size to assess substantial spatial variations at that scale.

Our results show that the trend in deformation band orientations are consistent from 3 m to 20 m scales in both sets (Fig. 10, Table 1). Dashed lines on Fig. 10 highlight variations that are similar in magnitude to the results of the sequentially bootstrapped means. As the sampling window moves toward the western end of the outcrop, the *spatial variations* in orientation are more variable at 3 m scales. At larger scales (10 m and 20 m), systematic spatial variations exist in both sets: in the NE-dipping set, the mean pole to the deformation band plane rotates progressively clockwise, whilst in the SW-dipping set the mean pole rotates from a steeper to a shallower plunge (Fig. 10).

4. Discussion

4.1. Spatial heterogeneity

Considering the entire population of orientations for the deformation bands, a traditional approach would be to determine the mean orientations of these two clusters and infer an Andersonian conjugate set of bimodal shear fractures as a best approximation. Our sampling strategy of a moving 1 m sampling window along a scanline with statistical analysis by bootstrapping, semivariogram plotting and hierarchical analysis demonstrate that such an interpretation is too simplistic. The sampling reveals a change in fracture geometry from single bands to band clusters westward with a related density change at about 20 m along the scanline. The bootstrapping and hierarchical analysis show a westward systematic steeping of inclination for the SW-dipping bands, and clockwise rotation of strike for the NE-dipping bands. The semivariograms show that these patterns of change are substantial for distances of at least 25 m with increasing differences in fracture

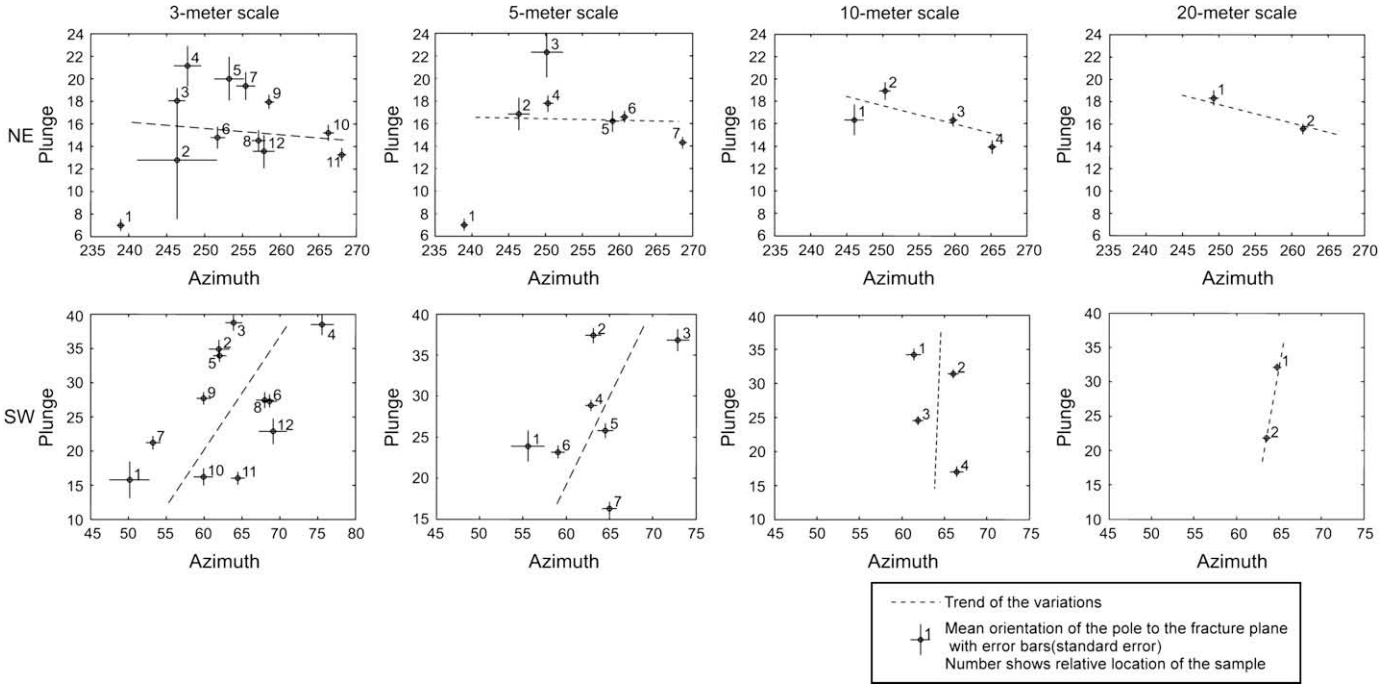

Fig. 10. Results of the hierarchical sampling of the mean deformation band orientation. Data points are the mean poles to the fracture planes for sample sizes of different areas mapped from the lower hemisphere projection to a 2D Cartesian coordinate frame. The sample number of each point indicates the relative location along the outcrop from east (lower number) to west (higher number). See Table 1.

Table 1
The relation of the sampling window size and the spatial location. Numbers in the first column are the relative location number as shown in the label to each point in Fig. 10. The last four columns show the corresponding real locations along the scanline at four different sampling scales.

No.	Scale			
	3 m	5 m	10 m	20 m
Hierarchical sampling				
1	0–3 m	0–5 m	0–10 m	0–19 m
2	4–7 m	5–10 m	10–20 m	19–38 m
3	7–10 m	10–15 m	20–30 m	
4	10–13 m	15–20 m	30–38 m	
5	13–16 m	20–25 m		
6	16–19 m	25–30 m		
7	19–22 m	30–35 m		
8	22–25 m			
9	25–28 m			
10	28–31 m			
11	31–34 m			
12	34–37 m			

orientation as distance between sampled fractures is increased. The combination of a systematic data collection protocol and three statistical techniques was needed to detect important patterns in the orientation data for the population of deformation bands. As a result, our field observations suggest that the cross-cutting deformation bands exhibit an orthorhombic symmetry. Such patterns are more consistent with 3D non-plane strains (Reches, 1978; Aydin and Reches, 1982; Reches and Dieterich, 1983), which are likely to be the main type deformation that occurs in the lithosphere (e.g. Dewey et al., 1998). Recent numerical modelling supports orthorhombic symmetry as a predictable consequence of the 3D interaction of mode I microcracks during the initial shear fracture nucleation and growth in various rock types (Healy et al., 2006a,b).

The deformation bands at the George Gill cliff section show a systematic, east to west change in orientations, which was revealed by applying bootstrapping and hierarchical analysis to a sample population gathered using 1 m sampling windows along a 40 m scanline. Fracture density increases sharply about 20 m westward from the east end of the cliff section. We propose that the density, orientation and fracture geometry changes with position are due to the presence of a NW trending normal fault dipping to the SW (Fig. 3 and 11). Equivalent changes in fracture orientations are observed in other natural systems as one passes from the wall rocks into the damage zones of larger faults (e.g. Faulkner et al., 2006) and lend support to the hypothesis that a larger fault lies close to the west end of the outcrop in George Gill.

4.2. Scaling issues

The scaling of fracture properties can in principle be determined quantitatively by comparing natural datasets with known, idealized distribution models, such as fractal, log-normal, exponential, etc. (Bonnet et al., 2001). Parameters such as fracture length, aperture and throw are measured in terms of length and as a result the size of the parameter can be directly related to the size of the sampling scale. Typically, the population of parameter sizes is plotted cumulatively versus the scale size for comparison to predictions from idealized distribution models. Power-law distribution and associated fractal geometry have yielded useful comparisons for fracture system characterization (Bonnet et al., 2001). Fracture orientation, on the other hand, has no direct intrinsic correlation to length. This situation leads to a problem in sampling this property in the field: how can an appropriate link between orientation and scale be created? Fractures form in a specific orientation with respect to the principal stress directions, but the orientation of the principal stress directions that one infers depends on the scale of observation (Tikoff and Wojtal, 1999). We therefore suggest that it is most appropriate to use the term 'granularity' to describe this hierarchical variation at different scales rather than the term 'scaling', because measurements of orientation are 'scale-isolated' and therefore have no direct relation to the length. Hence, to understand the distributions of fracture orientations at different scales, we define the window size independently (sampling or analysis granularity) from the type of measurements being taken (e.g. strike, dip, dip direction). Our approach here has been to change the size of the analysis window as an indirect way of representing the effect of a change of scale but we recognize that our dataset was collected at a single level of granularity. Nevertheless, we contend that averaging orientation data for a fracture population that display systematic spatial variations represents a type of spatial aliasing. This approach could lead to erroneous conclusions about the nature of the system and warrants further investigation. For example, such aliasing could mean that changes in fracture orientations across fault zones may be missed by coarse resolution fracture imaging methods such as seismic attribute mapping. Our example shows that orientation data are not necessarily scale invariant, such that sub-seismic scale fracture orientations could differ significantly from those at seismically imaged scales.

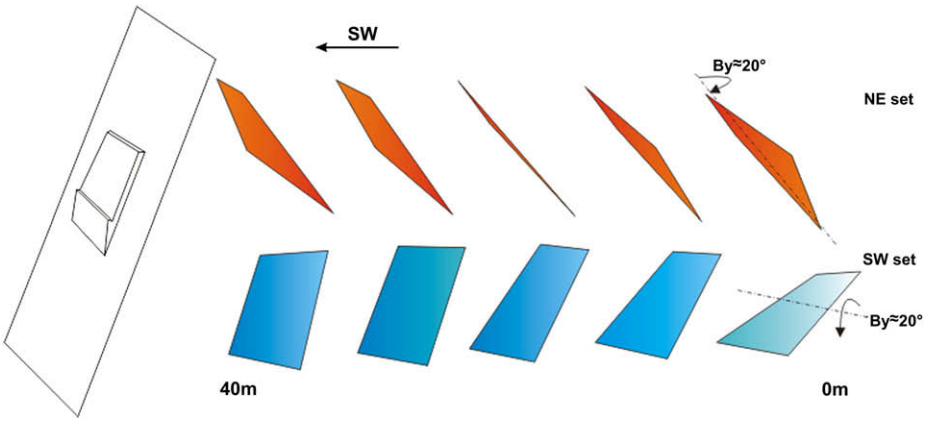

Fig. 11. Schematic diagram showing the observed systematic spatial variations in the orientations of the bulk NE- and SW-dipping deformation band planes along the cliff section. Postulated normal fault at west end of section is also shown.

Future work needs to define general statements that correlate the relationship between fracture orientations and fracture sizes at different scales. Qualitative field observations often suggest that, at outcrop-scales, little or no obvious relationship exists between fracture orientations and lengths. At a regional scale, however, this relationship may become more obvious, as major faults often appear to control the bulk orientation of nearby fracture zones. Such granularity in sampling the fracture orientations relating to the distribution of fracture size is an interesting issue that requires further study. It is not easy, however, to analyse the orientation datasets relative to their spatial positions, especially for datasets where the outcrops are of limited size, such as for the case study presented here. Ideally, it would be useful to quantify fracture orientations from outcrop to regional scales, because interpolation technique can be developed that estimates fracture orientation values based on limited observations. This approach applies not only to fracture networks on the surface, but also to those found in the subsurface. Flat pavements covering a large area, or long straight cliffs with simple fracture distribution patterns should represent ideal field areas to conduct such further studies.

5. Conclusions

The anastomosing deformation bands on the cliff at George Gill, Appleby, N. England show substantial spatial heterogeneity in their orientations. This heterogeneity is likely to have been controlled by the development of a NW–SE trending, SW-dipping normal fault adjacent to the cliff section. Multimodal fracture sets are developed locally and their orientation changes with position across the outcrop explaining the apparent change from bimodal to multimodal orientation distributions when downscaling from tens of metre-to-metre scales. Quantifying spatial variation in fracture orientation is key to understanding the geometry and connectivity of 3D fracture networks. The present study represents one of the first systematic accounts of the spatial heterogeneity of natural fracture orientations, and illustrates that a great deal more work remains if we are to be able to describe and accurately predict the complete fracture system in three dimensions.

Acknowledgements

Steve Laubach and Haakon Fossen are thanked for insightful reviews, and Bill Dunne for further review and thorough editing. J. Guo gratefully acknowledges receipt of a University of Durham ORS award and a Sir Kingsley Dunham Studentship. The authors thank Dave Healy for his contribution to this work, Steve Smith for help with the text, and Fabio Domingos for discussions.

References

Antonellini, M.A., Aydin, A., Pollard, D.D., 1994. Microstructure of deformation bands in porous sandstones at arches National-Park, Utah. Journal of Structural Geology 16 (7), 941–959.

Aydin, A., Johnson, A.M., 1978. Development of faults as zones of deformation bands and as slip surfaces in sandstone. Pure and Applied Geophysics 116 (4–5), 931–942.

Aydin, A., Reches, Z., 1982. Number and orientation of fault sets in the field and in experiments. Geology 10 (2), 107–112.

Barton, C.A., Zoback, M.D., 1992. Self-similar distribution and properties of macroscopic fractures at depth in crystalline rock in the Cajon Pass scientific drill hole. Journal of Geophysical Research-Solid Earth 97 (B4), 5181–5200.

Bonnet, E., Bour, O., Odling, N.E., Davy, P., Main, I., Cowie, P., Berkowitz, B., 2001. Scaling of fracture systems in geological media. Reviews of Geophysics 39 (3), 347–383.

Clegg, P., Bruciatelli, L., Domingos, F., Jones, R.R., De Donatis, M., Wilson, R.W., 2006. Digital geological mapping with tablet PC and PDA: a comparison. Computers & Geosciences 32 (10), 1682–1698.

Crampin, S., Mcgonigle, R., Bamford, D., 1980. Estimating crack parameters from observations of p-wave velocity anisotropy. Geophysics 45 (3), 345–360.

Dewey, J.F., Holdsworth, R.E., Strachan, R.A., 1998. Transpression and transtension zones. In: Holdsworth, R.E., Strachan, R.A., Dewey, J.F. (Eds.), Continental Transpressional Tectonics and Transtensional Tectonics. Geological Society Special Publication, vol. 135. Geological Society, London, pp. 1–14.

Efron, B., 1982. The Jackknife, the Bootstrap and other Resampling Plans. Pennsylvania, Philadelphia.

Faulkner, D.R., Mitchell, T.M., Healy, D., Heap, M.J., 2006. Slip on 'weak' faults by the rotation of regional stress in the fracture damage zone. Nature 444 (7121), 922–925.

Fisher, N.I., Lewis, T., Embleton, B.J.J., 1987. Statistical Analysis of Spherical Data. Cambridge University Press, Cambridge.

Fossen, H., Schultz, R.A., Shipton, Z.K., Mair, K., 2007. Deformation bands in sandstone: a review. Journal of the Geological Society 164, 755–769.

Gillespie, P.A., Howard, C.B., Walsh, J.J., Watterson, J., 1993. Measurement and characterization of spatial distributions of fractures. Tectonophysics 226 (1-4), 113–141.

Healy, D., Jones, R.R., Holdsworth, R.E., 2006a. New insights into the development of brittle shear fractures from a 3-D numerical model of microcrack interaction. Earth and Planetary Science Letters 249 (1–2), 14–28.

Healy, D., Jones, R.R., Holdsworth, R.E., 2006b. Three-dimensional brittle shear fracturing by tensile crack interaction. Nature 439 (7072), 64–67.

Isaaks, E.H., Srivastava, R.M., 1989. Applied Geostatistics. Oxford University Press, New York.

Johansen, T.E.S., Fossen, H., 2008. Internal geometry of fault damage zones interbedded siliciclastic sediments. In: Wibberley, C.A.J., Kurz, W., Imber, J., Holdsworth, R.E., Collettini, C. (Eds.), The Internal Structure of Fault Zones, vol. 299. Geological Society, London Special Publication 199, pp. 35–56.

La Pointe, P.R., Hudson, J.A., 1985. Characterization and interpretation of rock mass joint patterns. Geological Society of America Special Paper 199, 3–25.

La Pointe, P.R., 1993. Pattern analysis and simulation of joints for rock engineering. In: Judson, J.A. (Ed.), Comphrensive Rock Engineering: Rock Testing and Site Characterization, vol. 3, pp. 215–239.

Laubach, S.E., Olson, J.E., Gale, J.F.W., 2004. Are open fractures necessarily aligned with maximum horizontal stress? Earth and Planetary Science Letters 222 (1), 191–195.

Mardia, K.V., Jupp, P.E., 2000. Distribution on Spheres. John Wiley & Sons Ltd, Chichester.

Ortega, O.J., Marrett, R.A., Laubach, S.E., 2006. A scale-independent approach to fracture intensity and average spacing measurement. AAPG Bulletin 90 (2), 193–208.

Philip, Z.G., Jennings Jr., J.W., Olson, J.E., Laubach, S.E., Holder, J., 2005. Modelling coupled fracture-matrix fluid flow in geomechanically simulated fracture networks. SPE Reservoir Evaluation & Engineering 8, 300–309.

Reches, Z., 1978. Analysis of faulting in 3-Dimensional strain field. Tectonophysics 47 (1–2), 109–129.

Reches, Z., Dieterich, J.H., 1983. Faulting of rocks in three-dimensional strain fields 1. Failure of rocks in polyaxial, servo-control experiments. Tectonophysics 95 (1–2), 111–132.

Shipton, Z.K., Cowie, P.A., 2001. Damage zone and slip-surface evolution over mu m to km scales in high-porosity Navajo sandstone, Utah. Journal of Structural Geology 23 (12), 1825–1844.

Sigda, J.M., Goodwin, L.B., Mozley, P.S., Wilson, J.L., 1999. Permeability alteration in small-displacement in poorly lithified sediments: Rio Grande Rift, Central New Mexico. In: Haneberg, W.C., Mozley, P.S., Moore, J.C., Goodwin, L.B. (Eds.), Faults and Subsurface Fluid Flow in the Shallow Crust, Geophysical Monograph, vol. 113. American Geophysical Union, Washington, DC, pp. 51–68.

Tikoff, B., Wojtal, S.F., 1999. Displacement control of geologic structures. Journal of Structural Geology 21 (8–9), 959–967.

Underhill, J.R., Woodcock, N.H., 1987. Faulting mechanisms in high-porosity sandstones; New Red Sandstone, Arran, Scotland. In: Jones, M.E., Preston, R.M.F. (Eds.), Deformation of Sediments and Sedimentary Rocks. Geological Society Special Publication, London, vol. 29, pp. 91–105.

Versey, H.C., 1938. The petrography of the Permian rocks in the southern part of the Vale of Eden. Quarterly Journal of the Geological Society of London xcv, 275–298.

Wilson, R.W., McCaffrey, K.J.W., Holdsworth, R.E., Imber, J., Jones, R.R., Welbon, A.I.F., Roberts, D., 2006. Complex fault patterns, transtension and structural segmentation of the Lofoten Ridge, Norwegian margin: using digital mapping to link onshore and offshore geology. Tectonics 25 (4), TC4018.

Zadeh, L.A., 1979. Fuzzy sets and information granularity. In: Gupta, M., Ragade, R., Yager, R. (Eds.), Advances in Fuzzy Set Theory and Applications. North-Holland Publishing Co., Amsterdam, pp. 3–18.